

Single-particle subband structure of Quantum Cables

Z. Y. Zeng[‡], Y. Xiang, and L. D. Zhang

*Institute of Solid State Physics, Chinese Academy of Sciences, P.O. Box 1129, Hefei,
230031, P. R. China*

Abstract

We proposed a model of Quantum Cable in analogy to the recently synthesized coaxial nanocable structure [Suenaga et al. *Science*, 278, 653 (1997); Zhang et al. *ibid*, 281, 973 (1998)], and studied its single-electron subband structure. Our results show that the subband spectrum of Quantum Cable is different from either double-quantum-wire (DQW) structure in two-dimensional electron gas (2DEG) or single quantum cylinder. Besides the double degeneracy of subbands arisen from the non-abelian mirror reflection symmetry, interesting quasicrossings (accidental degeneracies), anticrossings and bundlings of Quantum Cable energy subbands are observed for some structure parameters. In the extreme limit (barrier width tends to infinity), the normal degeneracy of subbands different from the DQW structure is independent on the other structure parameters.

PACS numbers: 73.20.Dx, 73.61.-r, 03.65.Ge

I. INTRODUCTION

In recent years, the energy spectrum and transport properties of electrons in low-dimensional systems have received extensive attention. It is generally believed that quantum effects become more significant as the system dimensionality is reduced. In semiconductor, for example, confining electrons in a 2D plane, 1D wire or 0D dot gives rise to the obvious quantization of electron motion, which eventually results in some unusual transport and optical characteristics. With these interesting properties people can realize nanoscaled electronic devices with a variety of functions.

Since the prediction that 1D semiconductor quantum well wire can be of importance in high-speed-device applications[1], and their subsequent fabrication[2], there has been a great deal of interest in their transport and optical properties. Constantinou et al. [3] investigated the single-electron energy subbands of a solid cylindrical quantum wire in the absence and in the presence of an axial magnetic field. It is predicted [3] that the subband energy given by finite confining potential is reduced compared with the values given by infinite confining potential in the absence of magnetic effect. When a magnetic field applied along the axis of the wire, a minimum in the energies associated with carriers have negative azimuthal quantum number. If a solid cylinder is replaced by a hollow cylinder, Masale et al. [4] found that, the application of an axial magnetic field leads to a drastic modification in the subband spectrum. Makar et al.[5] demonstrated the oscillatory behavior of the density of states for a hollow cylinder under an axial magnetic field. Magneto-optical effects, collective excitation, transport behavior and other physical features in cylindrical quantum wires were also actively studied [6].

Coupled waveguide structures have long been the study subject of the optics and microwave community. Compared with the single waveguide system, coupled waveguide structure possesses some striking and unique features arising from the coupling between two waveguides, such as the enhanced quantum confined Stark effect [7] etc. These unique features are very useful in producing numerous devices including digital switches, multiplexers, and tunable filters [8]. To exploit the analogy between electromagnetic waves propagating along waveguides and electron transport in quantum wires, some theoretical investigations were devoted to the study of two coupled quantum wire used as field-effect directional couplers, energy filters, etc. [9]. In 1990, two coupled quasi 1D quantum wires device was fabricated by Alamo and Eugster, and its transport properties were

investigated both theoretically and experimentally. Later some groups calculated the ballistic conductance and magnetoconductance of such systems [11], and some interesting transport properties were displayed. Recently, Suenaga et al. [12] and Zhang et al. [13] synthesized successfully a new kind of quasi-one-dimensional composite structure termed as coaxial nanocable, in which two conducting cylindrical layers are separated by an insulating layer.

In the present work we propose a model of Quantum Cable consisting of two quantum cylinders coupled through a controllable potential barrier, motivated partly by the recent successful synthesis of coaxial nanocable [12,13]. Quantum Cable structure can be made either from the coaxial nanocable or from GaAs/AlAs system. For the former structure, if the energy-band structures of its two conducting layers are similar and the middle insulating layer is not thick enough to forbid electrons' tunneling, it can be viewed as a kind of Quantum Cable structure. For the later materials system, it is easier to fabricate and has close lattice matching. Depending on the Al concentration in $Al_{1-x}Ga_xAs$, its band gap can be changed continuously, thus the shapes of the barrier and well can be made almost to what one desires [Guo, JAP]. Therefore, Quantum Cable would be more easily fabricated from the GaAs/AlAs system. Moreover, multiple quantum cylinders and superlattice structure with cylindrical symmetry can also be available from the GaAs/AlAs systems. Quantum Cable is similar to but different from the DQW structure [10,11]. The similarities lie in that they are both coupled quantum-well structures. The major discrepancy between Quantum Cable and the DQW structure comes mainly from their different confining potential profiles and their symmetries. For DQW system, since extreme quantum limit is usually applied that only the lowest subband is populated, quantum confinement in one direction is enough to be taken into account. While for Quantum Cable system, its confining potential is symmetric with respect to Cable axis, and quantum confinement in two directions should be considered. This cylindrical symmetry introduces the two-fold degeneracies of eigen subbands, which consequently induces some unique optical and transport characteristics unexpected in the DQW system. Our numerical results show that the lowest (0,0) energy subband remains the ground subband either for single quantum cylinder (solid and hollow) or Quantum Cable irrespective of their structure parameters. Here we used the azimuthal quantum number n and radial quantum number l to label the subband (n, l) of Quantum Cable. As one of the structure parameters of Quantum Cable is varied with others being fixed, energy subbands of Quantum Cable exhibit interesting crossings (accidental degeneracies) and an-

ticrossings (repulsions), in the meantime, energy difference between neighboring subbands display inhomogeneous variation. Therefore, Quantum Cable can be regarded as a concrete example for studying the diabolical points in energy-level surface of real Hamiltonian system [] and Berry phase accompanying adiabatic changes []. If one adjust the coupling between the two quantum cylindrical wires, one can observe subband bundling before the extreme limit arrives (i. e. the width of the coupling barrier tends to infinity).

The paper is organized as follows. In Section II, we derived the formulas for calculating the energy subband in the single-electron approximation. Section III presents numerical calculations along with the associated analyses. A brief summary is given in Section IV.

II. MODEL AND FORMULATION

The proposed Quantum Cable comprises two coaxial cylindrical quantum wells. They are coupled through a tunable potential barrier, which allows for electron's tunneling between two cylindrical wells. The confining potential of Quantum Cable is very similar to a recently fabricated structure of coaxial nanocable and schematically shown in Fig. 1. The inside cylinder well has inner radius R_1 and outer radius R_2 , the outside cylinder has inner radius R_3 and outer radius R_4 . The height and width of the coupling barrier are U_B and R_B , respectively. It can be readily shown that the widths of the inside and outside cylinders are $R_{in} = R_2 - R_1$ and $R_{ou} = R_4 - R_3$. The electrons are free to move along the axis of Quantum Cable, whereas their motion in the radial direction is quantized. In the effective electron mass approximation, the Schrödinger equation governing the motion of electron with energy E read as

$$\left[-\frac{\hbar^2}{2m^*} \nabla^2 + U(\rho)\right]\Psi(\rho, \varphi, z) = E\Psi(\rho, \varphi, z), \quad (1)$$

where m^* is the electron effective mass and the confining potential of the Quantum Cable is

$$U(\rho) = \begin{cases} \infty, & \rho \leq R_1 \text{ or } \rho \geq R_4, \\ V_0, & R_2 \leq \rho \leq R_3, \\ 0, & \text{otherwise,} \end{cases} \quad (2)$$

In the cylindrical coordinates (ρ, φ, z) , the wave function $\Psi(\rho, \varphi, z)$ has the form $\chi(\rho)e^{in\varphi}e^{ik_z z}$, $n = 0, \pm 1, \pm 2, \dots$, where k_z is the axial wavevector. The radial wave function $\chi(\rho)$ satisfies the following

Bessel equation

$$\rho^2 \frac{d^2 \chi}{d\rho^2} + \rho \frac{d\chi}{d\rho} + \{[2m^*(E - U(\rho))/\hbar^2 - k_z^2]\rho^2 - n^2\}\chi = 0, \quad (3)$$

which has the following solutions

$$\chi(\rho) = \begin{cases} A_n J_n(k_1 \rho) + B_n Y_n(k_1 \rho), & R_1 \leq \rho \leq R_2, \\ C_n K_n(k_2 \rho) + D_n I_n(k_2 \rho), & R_2 \leq \rho \leq R_3, \\ F_n J_n(k_1 \rho) + G_n Y_n(k_1 \rho), & R_3 \leq \rho \leq R_4, \\ 0, & \rho \leq R_1 \text{ or } \rho \geq R_4, \end{cases} \quad (4)$$

where J_n is the Bessel function of first kind, Y_n the Bessel function of second kind and K_n, I_n are the modified Bessel functions, respectively, and

$$\begin{aligned} k_1 &= [(2m_1^*/\hbar^2)E - k_z^2]^{1/2}, \\ k_2 &= [(2m_2^*/\hbar^2)(U_B - E) + k_z^2]^{1/2}, \end{aligned} \quad (5)$$

are the wavevectors with m_i^* ($i = 1, 2$) being the electron effective mass in medium i . We now apply the standard effective-mass boundary conditions at $\rho = R_1, R_2, R_3, R_4$, which lead to the following equation satisfied by the eigen energy subbands:

$$\begin{aligned} &\frac{k_2}{m_2^*} f_1(k_1; R_1, R_2) \left[\frac{k_2}{m_2^*} F_1(k_1, k_2; R_2, R_3, R_4) + \frac{k_1}{m_1^*} F_2(k_1, k_2; R_2, R_3, R_4) \right] + \\ &\frac{k_1}{m_1^*} g_1(k_1; R_1, R_2) \left[\frac{k_2}{m_2^*} G_1(k_1, k_2; R_2, R_3, R_4) + \frac{k_1}{m_1^*} G_2(k_1, k_2; R_2, R_3, R_4) \right] = 0, \end{aligned} \quad (6)$$

where

$$\begin{aligned} f_1(k_1; R_1, R_2) &= J_n(k_1 R_2) Y_n(k_1 R_1) - J_n(k_1 R_1) Y_n(k_1 R_2), \\ g_1(k_1; R_1, R_2) &= J_n(k_1 R_1) Y_n'(k_1 R_2) - J_n'(k_1 R_2) Y_n(k_1 R_1), \\ F_1(k_1, k_2; R_2, R_3, R_4) &= [K_n'(k_2 R_3) I_n'(k_2 R_2) - K_n'(k_2 R_2) I_n(k_2 R_3)] \\ &\quad \times [J_n(k_1 R_4) Y_n(k_1 R_3) - J_n(k_1 R_3) Y_n(k_1 R_4)], \\ F_2(k_1, k_2; R_2, R_3, R_4) &= [K_n(k_2 R_3) I_n'(k_2 R_2) - K_n'(k_2 R_2) I_n(k_2 R_3)] \\ &\quad \times [J_n'(k_1 R_3) Y_n(k_1 R_4) - J_n(k_1 R_4) Y_n'(k_1 R_3)], \\ G_1(k_1, k_2; R_2, R_3, R_4) &= [K_n'(k_2 R_3) I_n(k_2 R_2) - K_n(k_2 R_2) I_n'(k_2 R_3)] \\ &\quad \times [J_n(k_1 R_4) Y_n(k_1 R_3) - J_n(k_1 R_3) Y_n(k_1 R_4)], \\ G_2(k_1, k_2; R_2, R_3, R_4) &= [K_n(k_2 R_3) I_n(k_2 R_2) - K_n(k_2 R_2) I_n'(k_2 R_3)] \\ &\quad \times [J_n'(k_1 R_3) Y_n(k_1 R_4) - J_n(k_1 R_4) Y_n'(k_1 R_3)], \end{aligned} \quad (7)$$

where $f'(x) = df(x)/dx$. Equation (6) may be solved numerically by employing the recursion relations satisfied by the Bessel functions outlined in Appendix. It should be pointed out that the formulas presented above are exact since no other approximation is made than the single-electron approximation.

III. RESULTS AND DISCUSSIONS

To start with, we study the subband spectrum of single quantum cylinder. For the convenience of comparison, throughout this work, we take $m_1^* = 5.73 \times 10^{-32}kg$, $m_2^* = 1.4m_1^*$, $m_3^* = m_1^*$, and energy in unit of $0.19eV$ and length in unit of angstrom. Fig. 2 shows the relation of subband energy with the solid quantum cylinder radius R_3 ($R_1 = R_2 = R_3$). The subband energy E_{nl} is related to the total energy via $E = E_{nl} + \hbar^2 k_z^2 / (2m^*)$ and is labeled by the azimuthal quantum number n and the radial quantum number l . For simplicity, calculations are performed by setting $k_z = 0$. As expected, the subband energy as well as the energy spacing between neighboring subbands decreases with the increase of the cylinder radius R_3 ; energy difference between adjoining subbands of lower-order is greater than that of higher-order. One can see from Fig. 2 that the lowest subband corresponds to $n = 0$, the next bound subband is an $n = 1$ subband. It is clear that for a given n , the value of R_3 at which a confined subband appears satisfies $J_n(k_1 R_3) = 0$. It so happens that the first $n = 0$ subband appears at a radius of about 40\AA . In Fig. 3 we present the calculated subband energy of a hollow quantum cylinder against the outside radius R_3 with a given inside radius $R_2 = 100\text{\AA}$, while the subband energy as a function of R_2 for a fixed $R_3 = 200\text{\AA}$ is given in Fig. 4. In two cases, $R_1 = 0$ and $V_0 = \infty$. It is obvious that the subbands with equal radial quantum number l converge as $R_3 - R_2$ approaches zero, with their energies having an $(R_3 - R_2)^{-2}$ variation. As the inside radius R_2 tends to zero while the outside radius R_3 keeps unchanged, we can observe an appreciable separation between subbands corresponding to different n but equal l quantum numbers. Crossings (accidental degeneracies) of some excited subbands is also seen for fixed R_3 and varied R_2 . However, the subband $(0, 0)$ remains the ground subband in either of the two cases. In addition, the subbands with nonzero azimuthal quantum number are doubly degenerate ($E_{nl} = E_{-nl}$) for both solid cylinder and hollow cylinder structures, the application of a magnetic field will violate such degeneration [4]. The double degeneracy of subbands is due to the fact that the mirror reflection across the plane parallel to Cable axis is non-abelian [14]. According to the

above analysis, our results obtained from Eqn. (6) is in very good agreement with Constantinou group's [3,4], which demonstrated the reliability of our formulation.

Now we inspect the energy subband structure of Quantum Cable. The variation of subband energy with the outer cylinder radius $R_3 - R_2$ is given in fig. 5 and with inner cylinder radius R_1 in Fig. 6. The parameters are chosen such that $V_0 = 0.19eV$, the barrier width $R_b = 25\text{\AA}$ and the inner cylinder radius $R_1 = 50\text{\AA}$ in Fig. 5 and the outer cylinder radius $R_3 - R_2 = 50\text{\AA}$ in Fig. 6. The subband (0,0) remains the ground subband and (1,0) the first excited subband whatever the value of the outer or inner cylinder radius. In Fig. 5, we also find, as $R_3 - R_2$ increases, the energy of some subband drops very slowly while that of the other subbands falls relatively rapidly. This leads to the crossings (accidental degeneracies) of some energy subbands: the second excited subband (0,1) as $R_3 - R_2 < 60\text{\AA}$ becomes the third excited subband with its crossed subband (2,0) becoming the second excited subband when $R_3 - R_2$ exceeds 60\AA ; as the outer cylinder radius $R_3 - R_2$ is further increased, it will turns into the other higher-order excited subband while the crossed subband is changed into the lower-order excited subband. Certainly, other higher-order subbands also exhibit such accidental degeneracy phenomenon as can be found in Fig. 5. In fig. 6, we find more interesting complicated accidental degeneracies: some excited subbands such as (0,1) and (1,1) becomes the lower-order excited subband first and then revives to the higher-order subband as the inner cylinder radius further increases. Another important feature is the inhomogeneous variation of energy intervals between adjoining subbands, which could be expected to result in some interesting optical and transport phenomena. It can be also expected that, the energy difference between neighboring subbands will be decrease with the further increase of either inner or outer cylinder radius.

Due to the quantum tunnel effect, electron's wavefunction will not be located within only one of the quantum cylinders, it would extend to the whole region of Quantum Cable. If the barrier height $V_0 \rightarrow \infty$ or barrier width $R_b \rightarrow \infty$, Quantum Cable will become the simple structure of two separated quantum cylinders. As the barrier height $V_0 \rightarrow 0$ or barrier width $R_b \rightarrow 0$, Quantum Cable turns into single solid quantum cylinder. It is therefore interesting to investigate how the coupling barrier influences the subband structure of Quantum Cable. In Fig. 7 we plot subband energy vs the barrier height V_0 and vs barrier width R_b in Fig. 8. With the increase of V_0 , subband energy grows up, energy spacing between neighboring subbands varies inhomogeneously, accidental

degeneracy of subbands is seen. As V_0 is further increased, we can observe accidental degeneracy of more than three subbands. While in the case of increasing barrier width, energies of some lowest subbands is lifted up while some falls off as R_b increase. This reflects the fact that the coupling of two cylinder wells becomes weak for large R_b . With the further increment of the barrier width, subbands energy tends to keep constant and some subbands tends to degenerate into one subband, while the ground subband does not degenerate with other subband. It is heuristic to compare this feature with that of 2D DQW structure. If the 2D DQW system consists of two identical wires, subband degeneracy only happens to two subbands with the same symmetry in the extreme limit ($R_b \rightarrow \infty$), and the ground subband will also degenerate with one of the subbands [15]. For 2D DQW with asymmetric confining potential, since the wave functions have no particular symmetry, no subband may cross and be degenerate. Though our calculating results are for Quantum Cable with two cylinders of the same radius, it is expected that subband crossing and degeneracy also occurs in Quantum Cable of different radius cylinders, because the same symmetry still preserve in the structure.

Finally, we give the number of available subbands for Fermi energy below 0.19 eV of a function of barrier height in Fig. (9a) and of barrier width in Fig. (9b). As expected, the available subband number exhibits an decreasing stepwise structure with the increase of barrier height and increasing stepwise profile as the barrier width increases. In addition, some comparatively narrow plateaus are also observed. This reflects the inhomogeneous variation of energy interval between adjoining subbands as the coupling parameter is varying.

IV. CONCLUSIONS

We studied the subband spectrum of Quantum Cable consists of a solid quantum cylinder and a hollow quantum cylinder, which are coupled through a potential barrier. The subband energy of solid quantum cylinder, hollow quantum cylinder and Quantum Cable are calculated. The results demonstrated a fact that Quantum Cable is an unique system to study quantum effects as bundling, accidental and normal degeneracy of levels. For single quantum cylinder or Quantum Cable, the subband (0,0) always keeps the ground subband whatever their structure parameters. Accidental degeneracies of subbands could be displayed in the case of hollow cylinder and Quantum Cable but does not appear in the subband spectrum of single solid quantum cylinder. This phenomenon might

be explained according to Wigner-Von Neumann theorem [16]: accidental degeneracy occurs only for the hermitian hamiltonian of no less than three changable parameters. As one of the parameters of Quantum Cable is varied, its energy subbands exhibit some interesting phenomena such as bundling, accidental and normal degeneracy, and inhomogeneous variation of energy separation between adjoining subbands. These features can be expected to be revealed in the optical spectrum observation of Quantum Cable. It is noted that accidental and normal degeneracy always occurs whatever the value of the inner-cylinder radius and outer-cylinder radius. It is contrast to the case of 2D DQW structure in which subband degeneracy occurs only for 2D DQW system with symmetric confining potential, since the wavefunctions have no particular symmetry in the asymmetric potential case. While for Quantum Cable structure, whatever the inner-wire radius and outer-wire radius, the symmetry is always preserved. Comparatively narrow plateaus are also observed in the plots of the available subband number as a function of the barrier height or width for a given Fermi energy, which will be reflected in the transport properties of electrons along the Cable axis. Subband spectrum of Quantum Cable with the application of magnetic field and other properties deserve further investigations.

ACKNOWLEDGEMENT

This work is supported by a key project for fundamental research in the National Climbing Program of China.

APPENDIX

In this appendix, we give some relations satisfied by various kinds of Bessel functions:

$$\begin{aligned}
 J_{-n}(x) &= (-1)^n J_n(x), & Y_{-n}(x) &= (-1)^n Y_n(x), \\
 I_{-n}(x) &= I_n(x), & K_{-n}(x) &= K_n(x), \\
 J'_n(x) &= J_{n-1}(x) - nJ_n(x)/x, & Y'_n(x) &= Y_{n-1}(x) - nY_n(x)/x, \\
 I'_n(x) &= I_{n-1}(x) - nI_n(x)/x, & K'_n(x) &= -K_{n-1}(x) - nK_n(x)/x
 \end{aligned}$$

where n is the natural number. The above equations are useful in evaluating the Bessel functions.

References

‡ E-mail address: zyzeng@mail.issp.ac.cn

1. Sakaki H 1980 Japan. J. Appl. Phys. **19** L735.
2. Petroff P M, Gossard A C, Logan R A and Wiegmann W 1982 Appl. Phys. Lett. **41** 635; Thornton T J, Pepper M, Ahmed H, Andrews D and Davies G J 1986 Phys. Rev. Lett. **56** 1198; Cibert J, petroff P M, Dplan G J, Pearton S J, Gossard A C and English J H 1986 Appl. Phys. Lett. **49** 1275; Temkin H, DoalnG J, Parish M B and Chu S N G 1987 ibid. **50** 413.
3. Constantinou N C and Ridley B K 1989 J. Phys.: condens. Matter. **1** 2283; Constantinou N C, Massale M and Tilley D R 1992 ibid. **4** 4499.
4. Massale M, Constantinou N C and Tilley D R 1992 Phys. Rev. B **46** 15432.
5. Makar M N, Ahmed M A and Awad M S 1991 Phys. Stat. Sol. (b) **167** 647.
6. Chen H, Zhu Y and Zhou S 1987 Phys. Rev. B **36** 8189; Huang F Y 1990 Phys. Rev. B **41** 12957; Wendler L and Grigoryan V G 1994 Pgy. Rev. B **49** 14531; Pokatilov E P, Klimin S N, Balaban S N and Fomin V M 1995 Phys. Stat. Sol. (b) **189** 433.
7. Kroemer H and Okamoto 1984 Jpn. J. Appl. Phys. **23** 970.
8. Yariv A 1985 Optical Electronics (HRW, New York).
9. del Alamo J A and Eugster C C 1990 Appl. Phys. Lett. **56** 76; Yang R Q and Xu J M 1991 Phys. Rev. B **43** 1699; Zhao P 1992 Phys. Rev. B **45** 4301; Xu G, Yang M and Jiang P 1993 J. Appl. Phys. **74** 6747.
10. Eugster C C, del Alamo J A, Rooks M J and Melloch M R 1992 Appl. Phys. Lett. **60** 642; Eugster C C, del Alamo J A, Melloch M R and rooks M J 1992 Phys. Rev. B **46** 10406; Eugster C C, del Alamo J A, Melloch M R and rooks M J 1993 ibid **48** 15057.
11. Wang J, Guo H and R. harris 1991 Appl. Phys. Lett. **59** 3075; Wang J, Wang Y J and R. harris 1992 Phys. Rev. B **46** 2420; Shi J R and Gu B Y 1997 Phys. Rev. B **55** 9941.
12. Suenaga K, Colliex C, Démoncy N, Loiseau A, Pascard H and Willaime F 1997 Science **278** 653.
13. Zhang Y, Suenaga K, Colliex C and Iijima S 1998 Science **281** 973.

14. Zeng J Y 1997 Quantum Mechanics (in Chinese) (Scientific Press).
15. Kamizato T and Matsuura M 1989 Phys. Rev. B **40** 8378; Morrison M A, Estle T L and Lane N F 1976 Quantum States of Atoms, Molecules, and Solids (Prentice-Hall Inc.).
16. wigner E P and von Neumann J 1929 J. Phys. Zeif **30** 467.

Figure Captions

Fig. 1 Schematic view of Quantum Cable structure.

Fig. 2 Lowest-order energy subbands of solid quantum cylinder as a function of radius.

Fig. 3 Lowest-order energy subbands of hollow quantum cylinder as a function of outside radius.

Fig. 4 Lowest-order energy subbands of hollow quantum cylinder as a function of inside radius.

Fig. 5 Lowest-order energy subbands of Quantum Cable as a function of outer-wire radius $R_3 - R_2$.

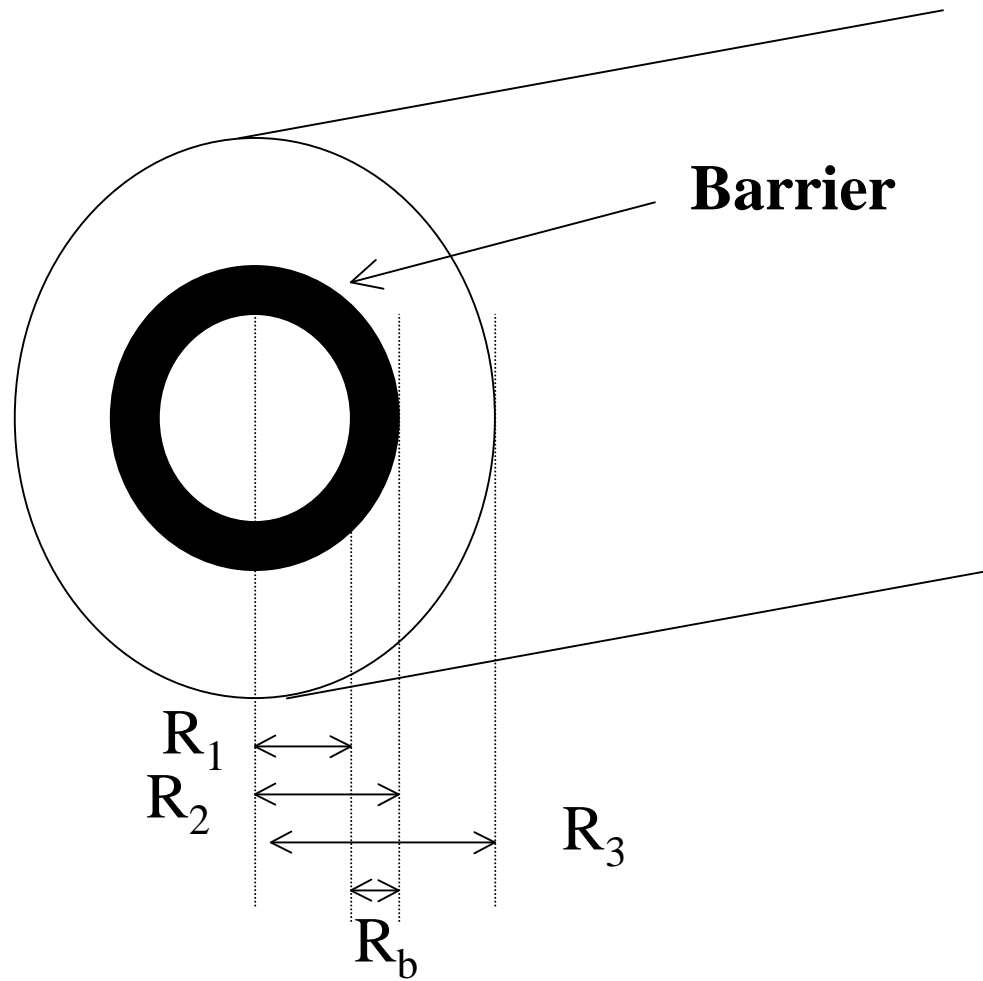
Fig. 6 Lowest-order energy subbands of Quantum Cable as a function of inner-wire radius R_1 .

Fig. 7 Lowest-order energy subbands of Quantum Cable as a function of the coupling barrier height V_0 .

Fig. 8 Lowest-order energy subbands of Quantum Cable as a function of coupling barrier width R_b .

Fig. 9 Number of available subbands for Fermi energy below 0.19 eV as a function of (a) coupling barrier height V_0 and (b) coupling barrier width R_b .

Fig.1 Zeng et al.



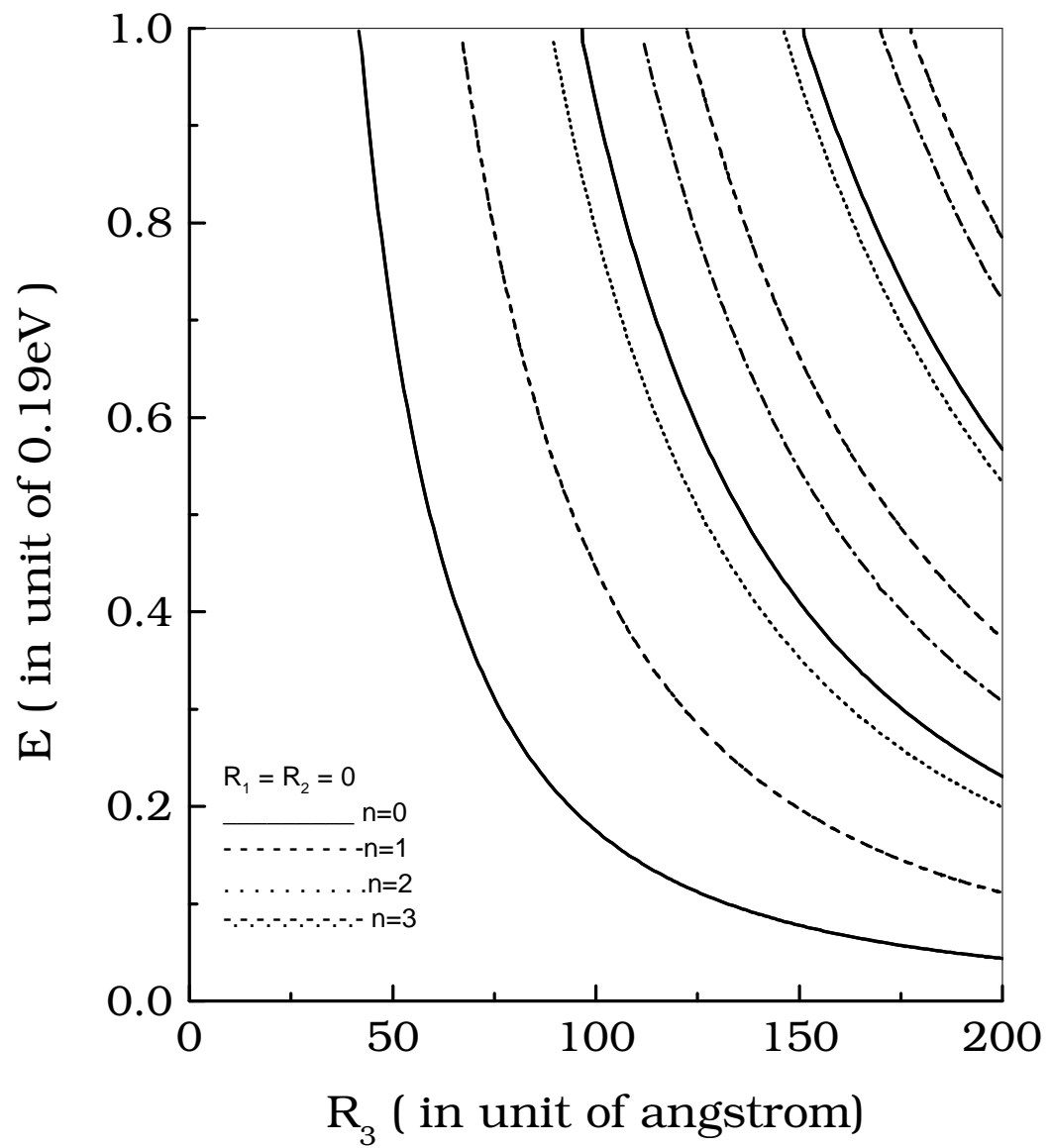


Fig. 2 Zeng et al.

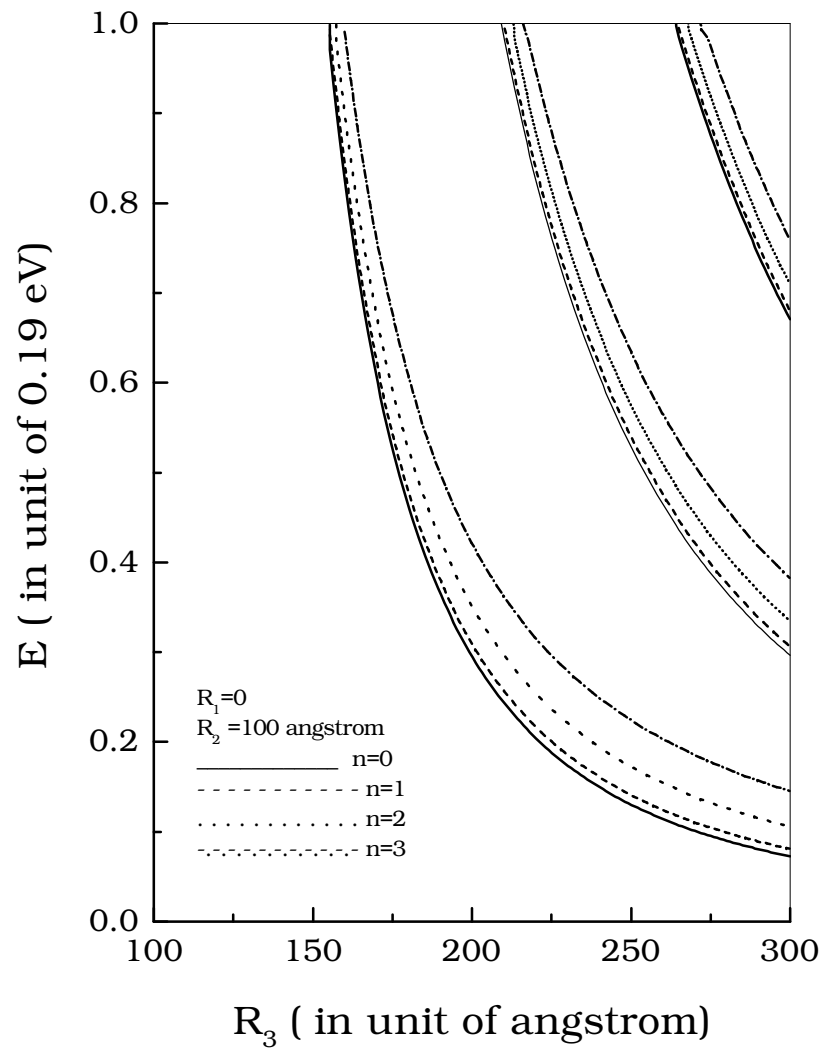


Fig. 3 Zeng et al.

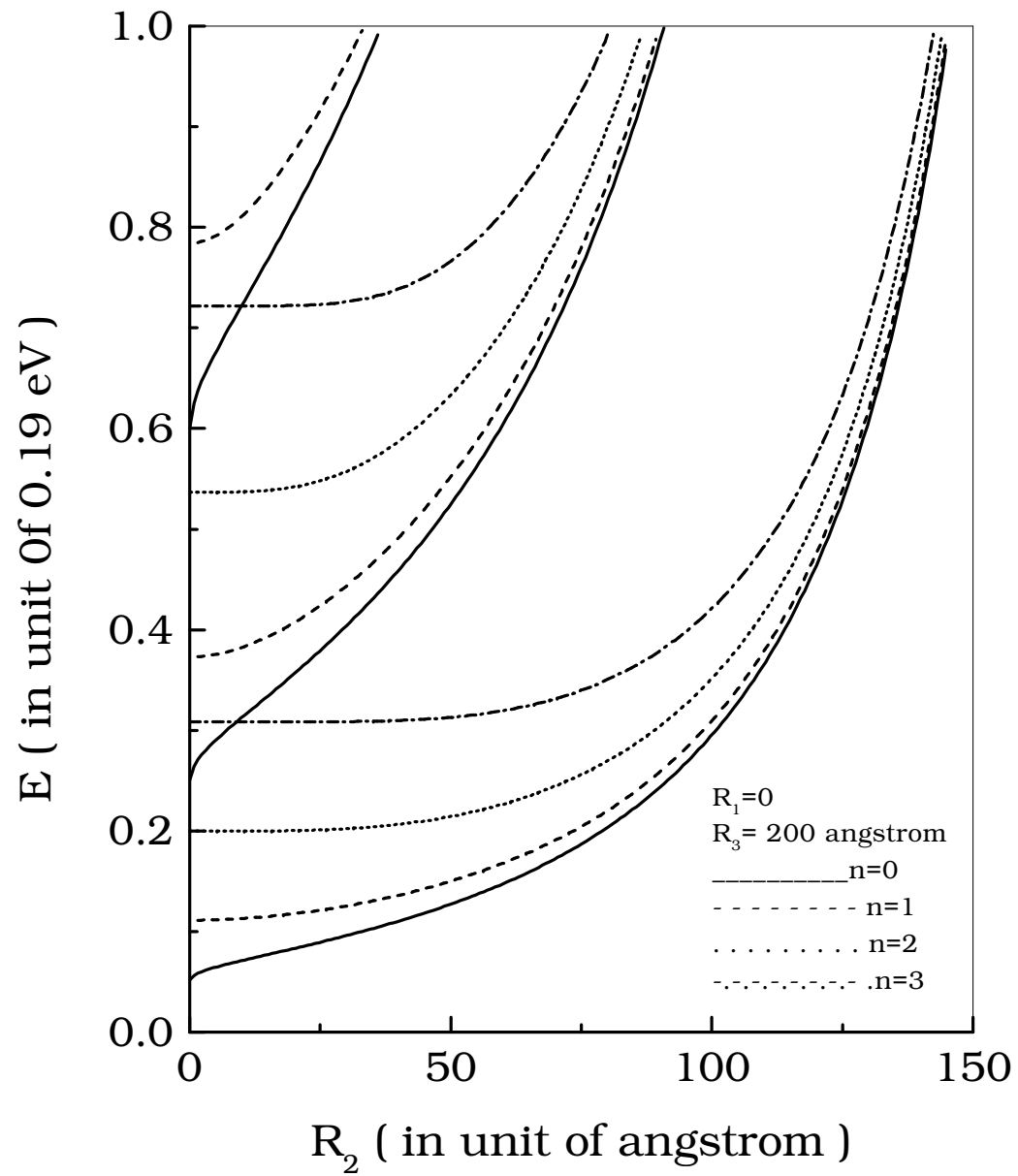


Fig. 4 Zeng et al.

Fig. 5 Zeng et al.

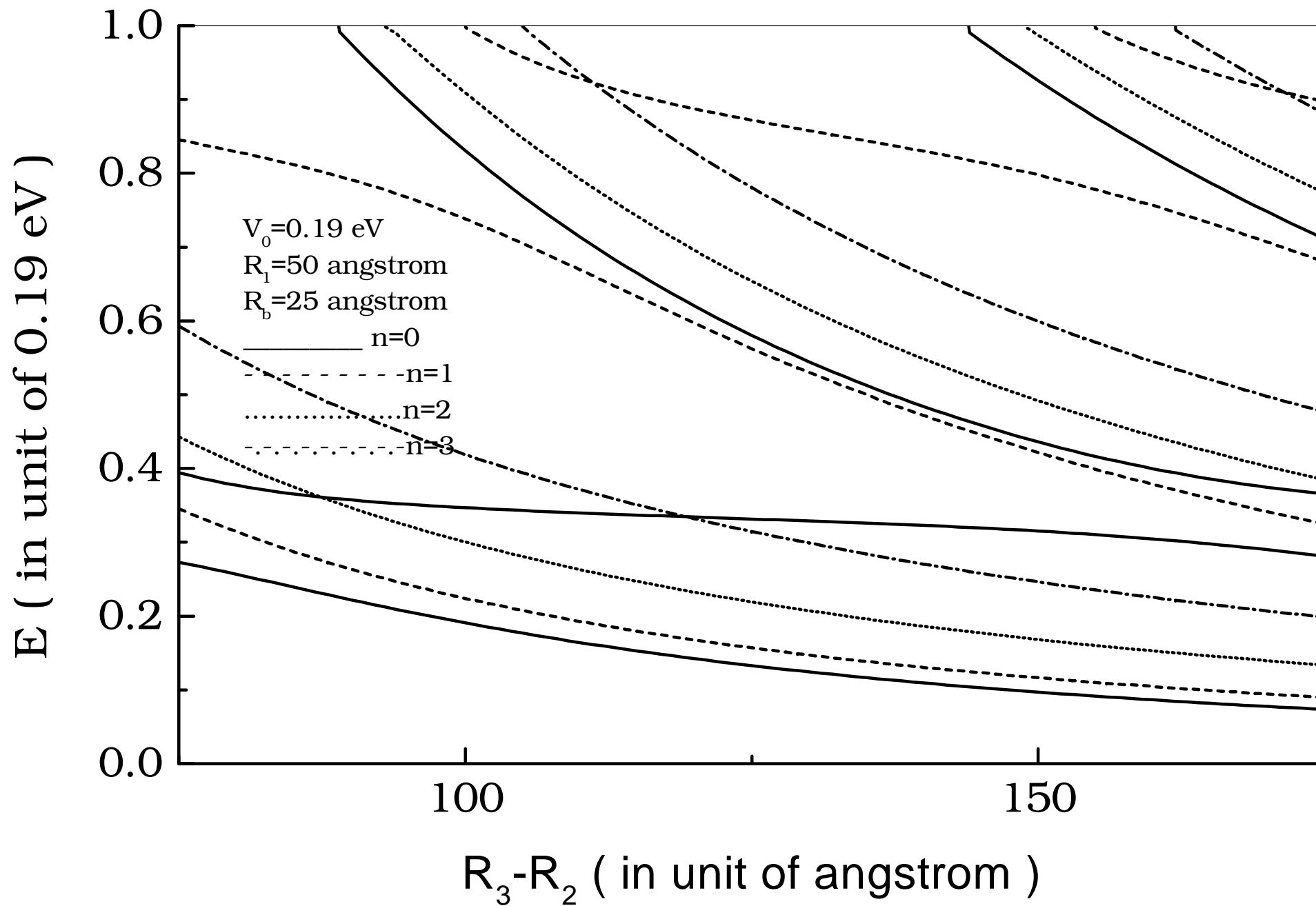


Fig. 6 Zeng et al.

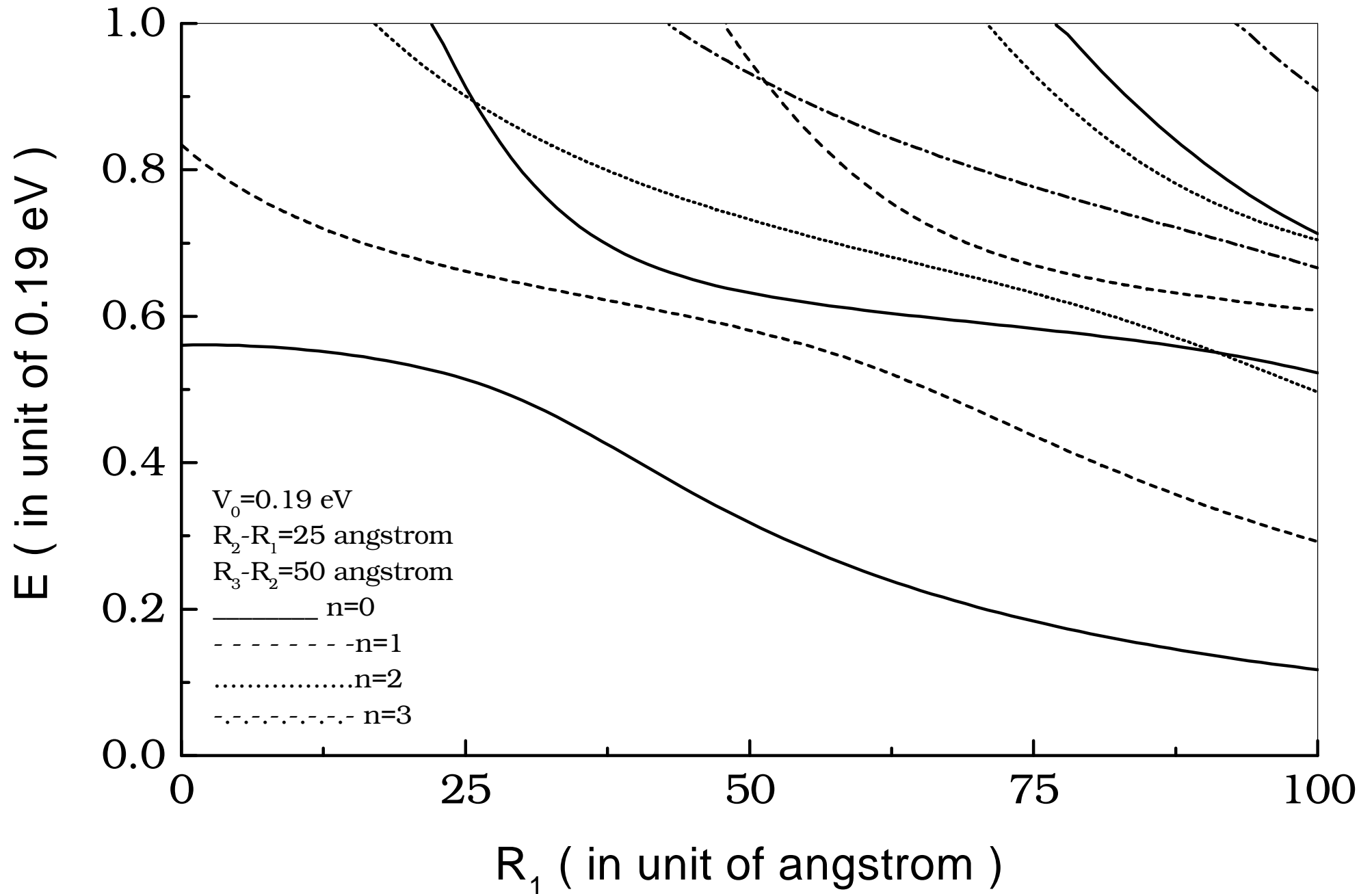


Fig. 7 Zeng et al.

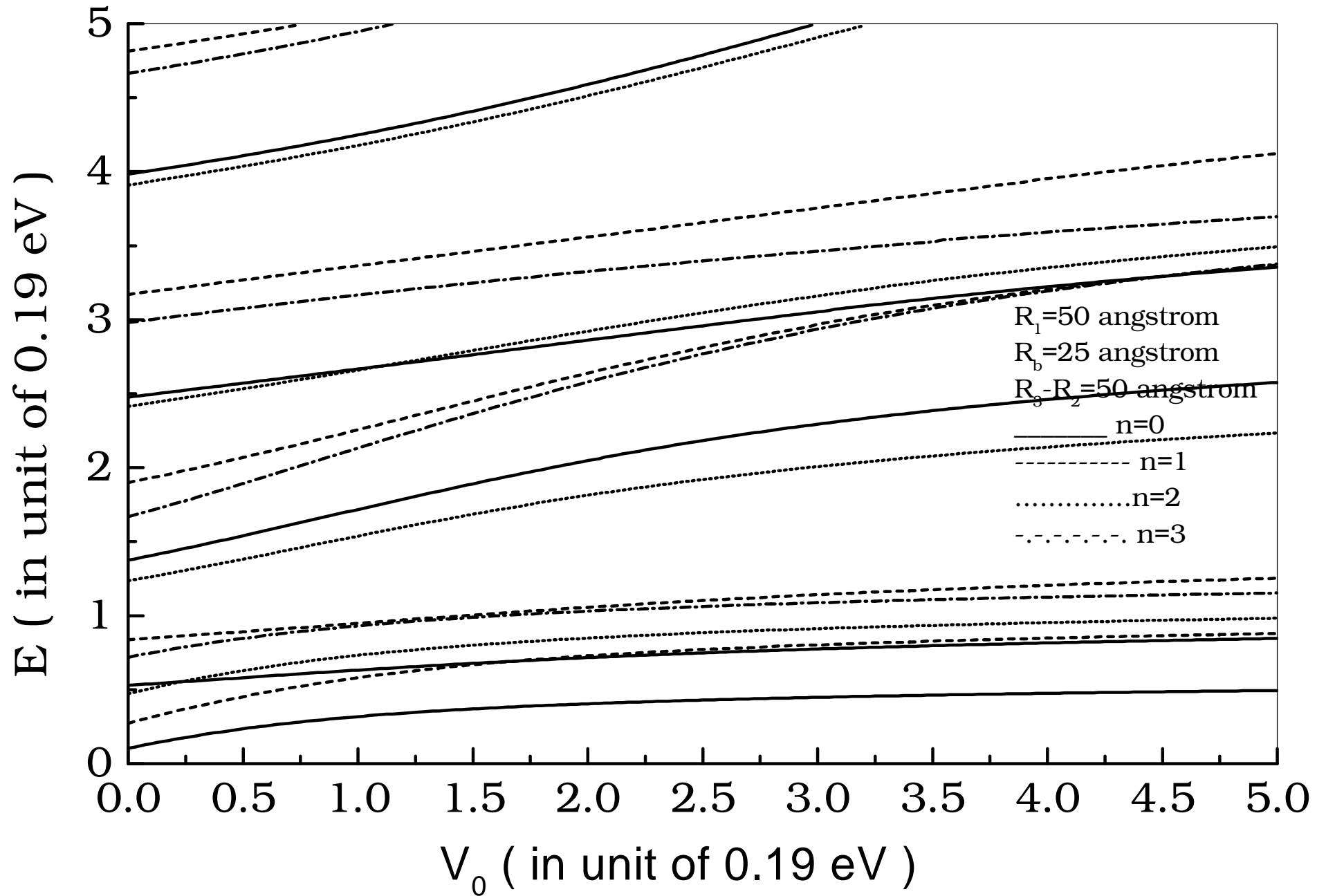


Fig. 8 Zeng et al.

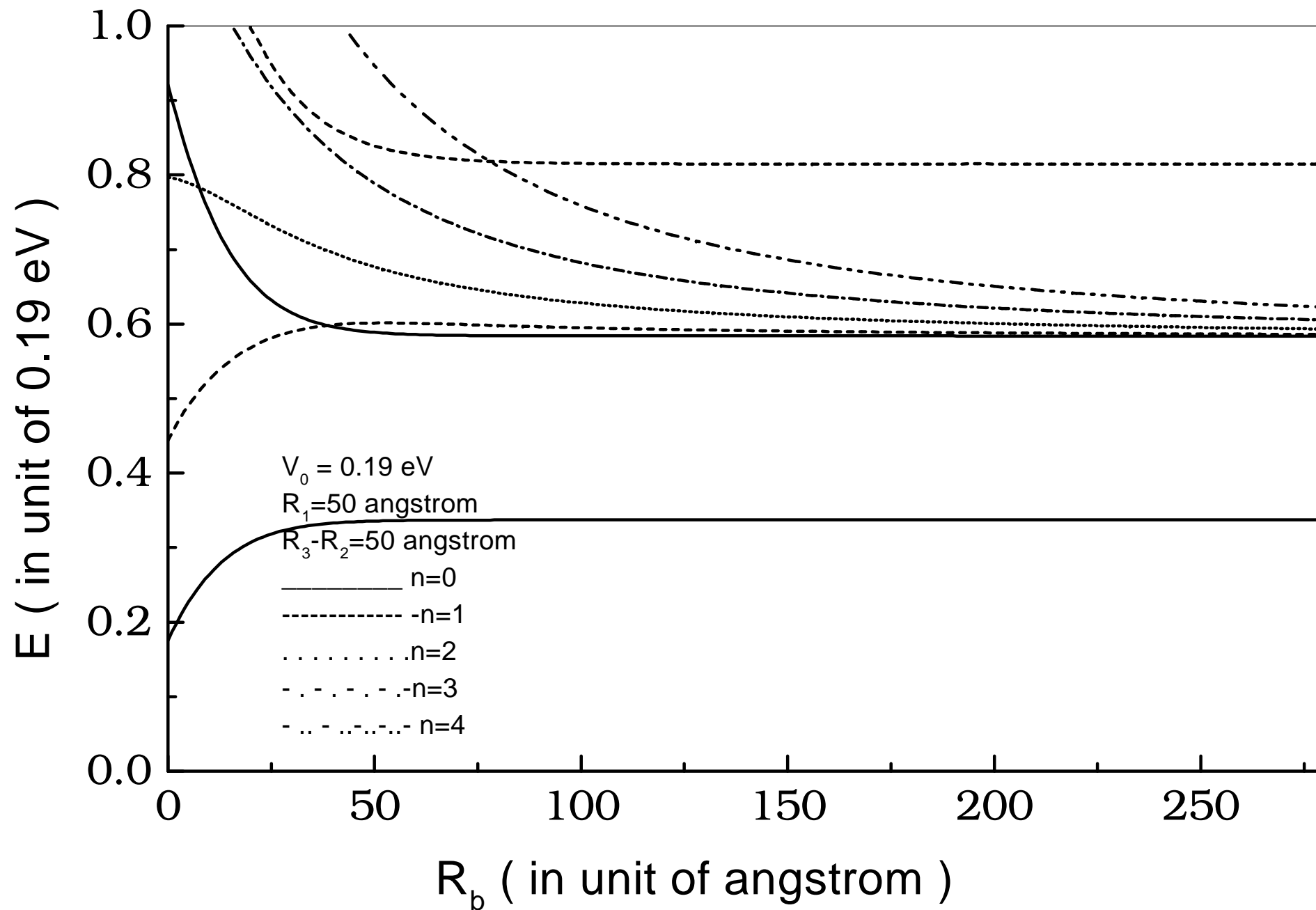


Fig. 9 Zeng et al.

